Inferring in-situ stress changes by statistical analysis of microseismic event characteristics

MELANIE GROB and MIRKO VAN DER BAAN, University of Alberta

Two commonly estimated fractal dimensions, called *b* and *D* values, represent statistical characteristics in the distribution of magnitude sizes (*b*) and spatial hypocenter locations (*D*) of microseismic events, respectively. We establish that the values of these two dimensions are related to specific stress regimes. Through the case study of a heavy-oil field drained using cyclic steam stimulation, we infer that the measured temporal variation in fractal dimension *b* is most likely due to significant changes in the local stress regime over a seven-month period, ranging from extensional faulting (fractures opening), via a strike-slip regime, to finally compressive faulting (fractures closing). The fracture dimension *D* indicates predominantly planar-to-spherical hypocenter spatial distributions in the first and last stages, but changes to a more linear-to-planar spatial pattern in the intermediate strike-slip regime when the vertical stress is anticipated to be in between the maximum and minimum horizontal stresses. These changes could be due to localized pore-fluid overpressure. A statistical analysis of the microseismic event locations and their magnitudes is therefore a useful method to understand reservoir geomechanics and thereby facilitate its management.

Introduction

Accurate information on the in-situ stress state is vital for sustainable reservoir management and development of successful drainage strategies as it determines the geomechanical behavior of the reservoir and overlying cap rock. It also impacts on drilling strategies designed to reduce the risk of borehole collapse and/or shearing, for instance, due to reservoir subsidence or fault reactivation caused by a changing stress field.

The most accurate stress information tends to be derived using borehole measurements. For instance, the minimum horizontal stress can be estimated through the fracture closure pressure from hydraulic fracturing or by leak-off tests; the maximum horizontal stress is evaluated from the breakdown pressure. Examination of fracture patterns in cores or well deformation also provides pertinent information. However, all borehole-derived measurements are representative only in the vicinity of the well and do not reveal how the stress regime might change spatially and temporally (e.g., during hydraulic fracturing of a tight-gas field or steam injection into a heavy-oil reservoir). There is therefore a need for developing other techniques to assess the in-situ stress regime, preferably with nondestructive, remote sensing capabilities.

Microseismic recordings are becoming increasingly more mainstream, in particular for unconventional reservoirs such as tight-gas or heavy-oil fields. Many interpretations tend to focus on the event locations, thereby ignoring other pertinent information contained in these recordings. Analysis of moment tensors and focal plane solutions reveals the underlying source mechanism of the recorded microseismic event. Individual source mechanisms yield constraints on the opening and closing of fractures and faults; and the local stress tensor can be obtained by analyzing a larger number of focal mechanisms (e.g., Gephart and Forsyth, 1984). Indeed, individual moment tensors should be similar for one cluster of events but will never be exactly the same; hence the local stress tensor might be slightly different from some individual moment tensors. Although this approach is almost routinely invoked in global seismology, it is less often applied to microseismic recordings, predominantly due to limitations introduced by the acquisition geometries (e.g., a single observation well is the norm).

In this paper, we will employ an alternative approach and demonstrate how a statistical analysis of commonly estimated microseismic event characteristics can also help infer constraints on the in-situ stress field. We will look in particular at the shape of the event cloud, as well as the magnitude-frequency distribution. Both the event position and magnitude are routinely estimated, thus offering a versatile and inexpensive analysis tool.

Fractal dimensions *b* and *D*

Gutenberg and Richter (1944) inferred the fractal nature of

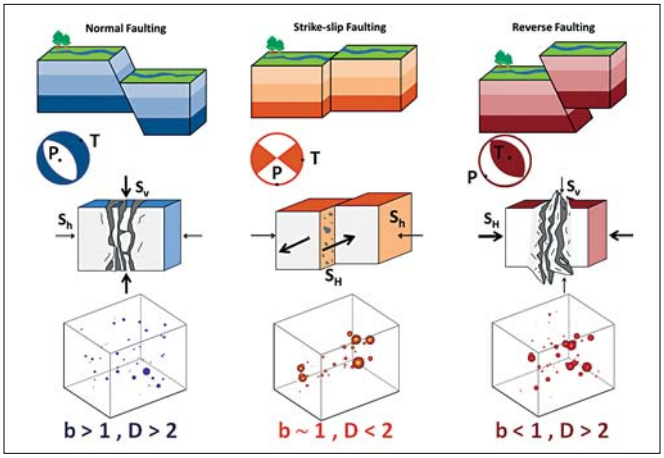

Figure 1. *The different stress regimes (top), the associated rock deformation (center), and resulting microseismicity (bottom). The little balls under the diagrams at the top represent the focal mechanisms for each stress regime. P and T denote the pressure axis (maximum compressive stress direction) and the tension axis (minimum compressive stress direction), respectively. The left column depicts the extensional regime with the associated normal faulting, opening of fractures, and large amount of small-magnitude events that are evenly distributed spatially. The strike-slip regime (center column) creates planar fractures which produce an even proportion of small-to-large events during slipping oriented along a plane. The right column shows the compressive stress regime which implies reverse faulting and closing of fractures with many large-magnitude events evenly distributed in space. In the center row, S_h and S_H represent, respectively, minimum and maximum horizontal stress, and S_v indicates vertical stress. Arrow thickness is proportional to stress magnitude. On the bottom row, event circle size is proportional to magnitude.*

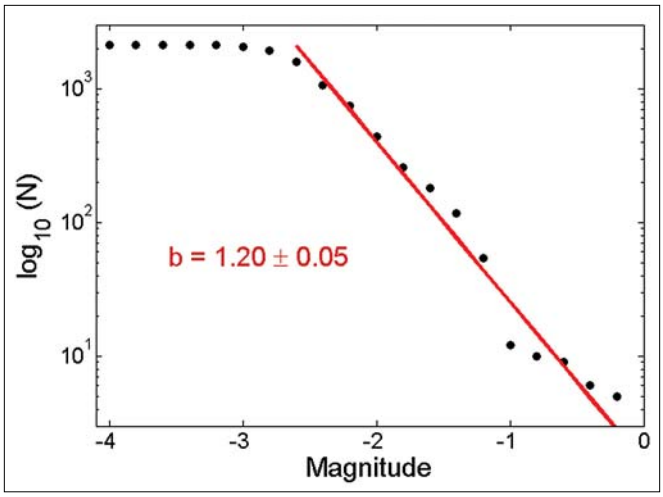

Figure 2. *Event-size distribution for a heavy-oil data set. The size distribution follows a power law with a b-value of 1.20.*

earthquake-size distributions. Mogi (1962) and Scholz (1968) demonstrated the same fractal distribution for seismicity generated in laboratory experiments on rock fracturing. Since then many other fractal relationships have been inferred from studies of spatial and temporal distributions of seismic events.

As a result, fractal dimensions are defined to characterize rock fracturing, ranging from the microscopic level encountered in laboratory experiments to the macroscopic level of earthquakes. Variations in these fractal dimensions can give insights into the underlying fracturing mechanisms operating at the heart of the rock failure. Here we focus mainly on two specific fractal dimensions, called the *b* and *D* values, which give a clue on the distributions in magnitude size (*b*) and spatial hypocenter locations (*D*), respectively.

The *b*-value is the exponent of the Gutenberg-Richter power law relation indicating the frequency of occurrence *N* of earthquakes of a magnitude m larger than a value *M*, that is:

$$\log\left(N\left(m > M\right)\right) = a - bM$$

A high *b*-value indicates a relatively large proportion of small earthquakes occur, while small *b*-values mean larger events happen relatively more often. As the size of an event usually depends on the amount of slip on the fault or fracture, *b*-values also give an idea about the distribution of slip magnitudes.

Schorlemmer et al. (2005) find a correlation between the *b*-value and the tectonic stress regime. The highest *b*-values (>1) are for normal faulting events, intermediate values (around 1) for strike-slip earthquakes and the lowest *b*-values (<1) for thrust events (Table 1). As normal faults tend to occur under lower horizontal stresses than thrust faults, these changes in the *b*-value are proportional to vertical minus horizontal differential stress. Further evidence for this comes from lab experiments and observations in mining rock bursts.

The size of *b*-values derived from analysis of acoustic emissions occurring during rock failure experiments in the lab are also observed to be proportional to the vertical minus horizontal differential stress (Liakopoulou-Morris et al., 1994). Amitrano (2003) observes an increase in *b*-values as the vertical minus horizontal differential stress decreases. Urbancic et al. (1992) compute *b*-values and stress release estimates for a rockburst experiment and again find *b*-values inversely correlated to stress.

An intuitive explanation as to why high *b*-values are linked to normal (extensional) faulting (Table 1) is that slip occurs more easily when materials are pulled apart, thus giving rise to many small earthquakes and fewer larger ones (high *b*-value). Conversely, asperities on fault planes can become significant obstacles to slip in a compressive regime (reverse faulting), thus leading to relatively more large magnitude events (low *b*-value).

A second statistical variable of interest is the fractal dimension *D*, characterizing the spatial distribution of hypocenters. It too is likely related to changes in the stress field as well as the spatial distribution of damage and brittle failure. It is quantified using the spatial correlation integral method proposed by Grassberger and Procaccia (1984). This integral is defined as

$$C(r) = \frac{2}{N(N-1)N(R<r)}$$

where N is the total number of events and $N(R<r)$ is the number of pairs of events separated by a distance R smaller than r. If the distribution is fractal, the correlation integral will follow a power law distribution with distance r:

$$C(r) \propto r^{D}$$

where *D* is the fractal dimension (also called correlation coefficient).

D is equal to 0 for a point, 1 for a line, 2 for a plane, and 3 for a sphere. So *D* gives an indication of the spatial shape distribution of event locations. Non-integer values reveal a clustering of the events closest to the shape described by the nearest integer value. *D*-values need not be stationary over time. If *D* decreases from 3 to 2 over time, it means that events that are first randomly distributed in a sphere gather along a fault plane. For instance, in rock fracturing experiments, acoustic events are randomly distributed during the first stage (*D*~3) and progressively cluster around a plane forming the macrofracture that eventually breaks the sample (Hirata, 1987; Lockner, 1993) giving *D*~2.

The fractal dimension D is also related to the irregularity of stress and strength distributions or fracture stiffness distribution, and thus reflects the structure of the fault network. *D*-values may also be linked to the local or regional stress regime. For instance, hydraulic fracturing in strike-slip regimes tend to produce microseismic event locations confined to linear structures (*D*~1) or vertical planes (*D*~2), as seen for instance in both the Carthage Field treatments in the Upper Cotton Valley Formation in Texas, USA (Ruthledge, 2004) or the Canyon Sands gas fields, also in Texas (Fischer, 2008). This is not the case in normal or reverse faulting regimes where hypocenters tend to follow more planar to spherical distributions (*D*>2).

Figure 1 summarizes anticipated fractal dimensions *b* and

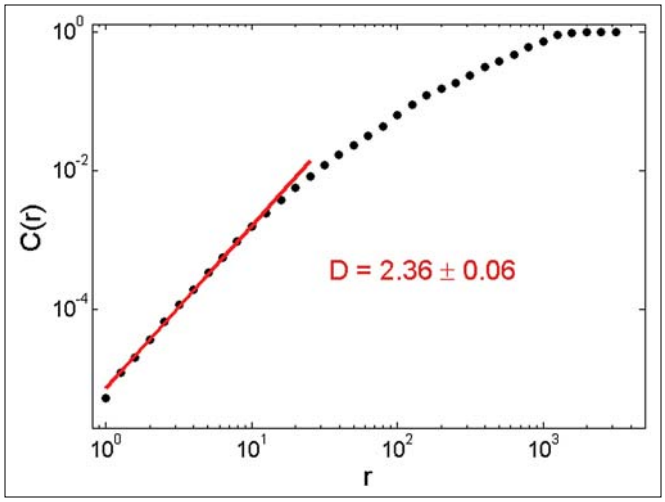

Figure 3. *Correlation integral for a heavy-oil data set. The average spatial fractal dimension D equals 2.36 indicating a predominantly spherical event cloud. The distance r is in meters.*

D to the existing stress regime and anticipated deformation at the fracture scale. Normal faulting belongs to the extensional regime which implies some opening of fractures. This process usually comes with lots of small-magnitude events which are spread over the entire stressed area resulting in *b* and *D* values in excess of 1 and 2, respectively. Reverse faulting, however, leads to closing of fractures because of compression such that many more stronger and spherically distributed events occur, hence the low *b* values and high *D* values as depicted in Figure 1. The strike-slip regime is characterized by a more planar geometry and a better proportionality between small and large events, which is represented by *b* and *D* values around 1.

Case study

To illustrate the use of these simple statistics to describe the stress regime in a reservoir, we compute the average *b*- and *D*-values for a microseismic data set acquired above a heavy-oil field. The heavy-oil reservoir is drained using cyclic steam stimulation. 2132 events were recorded from September 2009 to March 2010. Prior to December 2009, only injection occurred in the field; then a combined injection/production strategy was adopted.

The frequency-size distribution obtained using all events is plotted in Figure 2. This distribution follows a power law with an exponent b equal to 1.20. The plateau for magnitudes less than –2.6 indicates that many smaller events are not successfully recorded, so the *b*-value is calculated only over the reliable magnitude-distribution part of the catalog. According to Table 1, the local stress regime is of type $S_v > S_H > S_h$ and thus most likely to lead to normal faulting (extension). The occurrence of extensional faulting is plausible in the areas above the steam cloud.

Figure 3 shows the correlation integral (plotted on log axes) used to evaluate the spatial fractal dimension *D* which is again estimated over the linear part of the curve and equals 2.36, meaning the events are distributed rather evenly (spherically) in space. The change in the slope of the curve after a distance *r* of 10 m is a sign of depopulation which could lead to a bias in the statistics, so the slope value for *D* is computed only over the first part of the distribution consistent with a log linear expectation from the spatial correlation integral relationship between *D* and *r*.

Given the large number of recorded events, an analysis of temporal variations in the *b*- and D-values can be made. Figure 4 represents the variations of the *b*-value in time from September 2009 to March 2010. The *b*-values are computed over 300 events with a moving window shift of 30 events. Ranges are defined on the number of events and not on time to reduce potential bias in the estimated statistical value.

Three different stages could be seen in Figure 4, highlighted by colored ellipses. The *b*-values are high at the beginning (b>1.1), followed by a decrease to intermediate values (b~1), and end at a low level (b~0.65) after mid-January 2010. These variations indicate a change in the stress state of the reservoir from extension (i.e., opening of fractures) to compression (closing of fractures) with an intermediate stage of mostly strike-slip events (Table 1 and Figure 1). It would also mean that horizontal stresses were originally smaller than the vertical stress ($S_v > S_H > S_h$) but dominated in the end ($S_H > S_h > S_v$). This scenario is plausible from the initial phase of steam injection (extension phase) until the start of production (compression phase).

Figure 5 represents the temporal evolution of fractal dimension *D* for the same period and with the same parameters for the moving window as employed for computing the *b*-values. The variations in dimension *D* are more pronounced than those of the *b*-values. Dimension *D* varies mostly between 2 and 3, indicating a spherical distribution of events, except in December 2009 when the *D*-value dropped to 1. This period corresponds to a change in injection/production strategy in the reservoir. Such changes in injection/production can alter the stress state in the reservoir, resulting in a different clustering of events at places where the variations are the highest. A relaxation phase follows and events return to a more uniform or spherical distribution in January 2010.

D-values less than 2 are characteristic of a strike-slip regime, where planar to linear event clouds are anticipated (Table 1 and Figure 1). Figure 5 thus confirms the conclusions drawn from the observed b-values (Figure 4) that a strike-slip regime is dominant around December 2009. Our observations thus point to a model where initial extension and opening of cracks is followed by a strike-slip regime likely dominated by crack shearing, and ultimately a compressive stress field with cracks closing.

Rozhko et al. (2007) developed numerical simulations to

b-value	Stress regime	Fault type
$b < 1$	$S_H > S_h > S_v$	Reverse (compressive)
$b = 1$	$S_H > S_v > S_h$	Strike-slip
$b < 1$	$S_v > S_H > S_h$	Normal (extensional)

Table 1. *Links between b-values, stress regime, and dominant faulting type, based on work by Schorlemmer at al. (2005). S_H = maximum horizontal stress. S_h = minimum horizontal stress. S_v = vertical stress.*

understand the interactions between pore-fluid overpressure and failure patterns in rocks and their results show different failure patterns, either with tensile or shear mode, depending on the initial conditions, the geometry, and the material properties. We therefore postulate that localized pore-fluid pressure can affect the stress regime and hence be responsible for the changes we see in our analysis.

Discussion

The three most likely factors that control the geomechanical behavior of a reservoir are the local stress regime, pre-existing fractures (and other zones of weaknesses), and the actual rock properties (e.g., whether they are more ductile or brittle, and their Young's modulus or Poisson's ratio and thus their Lamé parameters). Microseismic monitoring records where brittle failure occurs and can thus reveal a wealth of useful information on the in-situ stress state, fracture distributions, and rock properties. This can be achieved using both a statistical and deterministic analysis of event hypocenters and magnitudes.

In this paper, we focus on a statistical approach analyzing both the fractal dimension of the spatial distribution in hypocenters and the magnitude-size occurrence using the well-known fractal dimensions b and D. Computing these fractal dimensions is a simple procedure given a sufficiently large microseismic data set and can reveal pertinent information on the in-situ stress regime.

Our analysis is largely based on the observations of Schorlemmer et al. that the fractal dimension b is linked to the stress regime. Their result is obtained, however, using the focal mechanisms of regional and global earthquakes which are dominated by double-couple sources representing slip on a fault plane. It remains to be established if Table 1 is also appropriate when more complex rupture mechanisms occur, involving for instance significant volume (opening or closing) changes. This is important since microseismic events observed during tight-gas hydraulic fracturing and possibly in other unconventional fields are thought to have significant non-double couple source mechanisms (Baig and Urbancic, 2010)

On the other hand, the same observations seem to resolve an existing ambiguity on potential relationships between measured b and D-values. Some authors do not detect any correlation between both fractal dimensions in their analyses of data whether at microscopic or macroscopic scales (Hirata et al., 1987). Other authors find a positive correlation between these two values (Huang and Turcotte, 1988), whereas others observe a negative correlation (Henderson et al., 1992; Amitrano, 2003). Many authors agree, however, on the importance of fracture interactions which may determine the sign of the correlation coefficient between b and D values (Huang and Turcotte, 1988; Henderson et al., 1992; Helmstetter et al., 2005). Our observations suggest the sign and presence of any correlations between both fractal dimensions are determined by the underlying stress regime and its spatial and/or temporal evolution. In our case, the sign change is mainly due to the change in D-value, but only because the b-value keeps on decreasing.

Our analysis is complementary to results obtained via moment tensor inversions which attempt to infer the actual fracture mechanisms. However, moment tensor inversions require signals with a high signal-to-noise ratio and a sufficiently large aperture in the acquisition geometry (Eaton and Forouhideh, 2010), conditions that are not often achieved during the monitoring of steam injection in a gas/oil field or tight-gas hydraulic fracturing. Usually only a small number of events can thus contribute to such a study. The described statistical analysis of the fractal b- and D-dimensions can therefore act as a complementary tool to cross-check the results obtained using moment-tensor inversions.

An important difference between the moment tensors and the b and D statistics is that the latter will give a global insight about the principal stress directions and thus the most likely geomechanical behavior of the reservoir, whereas a moment tensor is linked to the rupture process of a single event. Furthermore, it is not feasible to invert for the underlying stress regime using a single focal mechanism (McKenzie, 1969). The statistical analyses can be performed on a distinct cloud of events and for which moment tensor inversions are also available, thereby permitting an in-depth scrutiny of a particular area. The two methods may therefore be used correlatively.

Conclusion

Statistical analysis of the spatial distribution in hypocenters and the magnitude-size by computing the fractal dimensions b and D provide constraints on the in-situ stress regime surrounding a reservoir. Computing these fractal dimensions is a simple procedure given a sufficiently large microseismic data set.

The b-values are related to the distribution of fault lengths and amount of slip versus the number of events via the event magnitude. Analysis of the b-values therefore contains pertinent information on the amount of internal deformation (e.g., due to hydraulic fracturing) and thus potential increase in permeability via enhanced fracture densities.

The fractal dimension D reveals the shape of the event cloud (line, plane, or sphere) and is hence useful to evaluate the shape of the damage zone. Thus b and D values yield the shape of the damage zone and the fracture distribution inside this zone.

Our analysis of microseismicity occurring in a heavy-oil field drained using cyclic steam stimulation implies that the measured temporal variation in fractal dimension b results from a strong variation in local stress regime over a seven-month period, ranging from extensional faulting (fractures opening), via a strike-slip regime, to finally compressive faulting (fractures closing). The fracture dimension D indicates predominantly planar-to-spherical spatial hypocenter distributions in the first and last stage, but changes to a more linear-to-planar spatial pattern in the middle strike-slip regime when the vertical stress is anticipated to be in between the maximum and minimum horizontal stress. A statistical analysis of the microseismic event locations and their magnitudes therefore contains a wealth of information to facilitate reservoir management. TLE

References

Amitrano, D., 2003, Brittle-ductile transition and associated seismic-

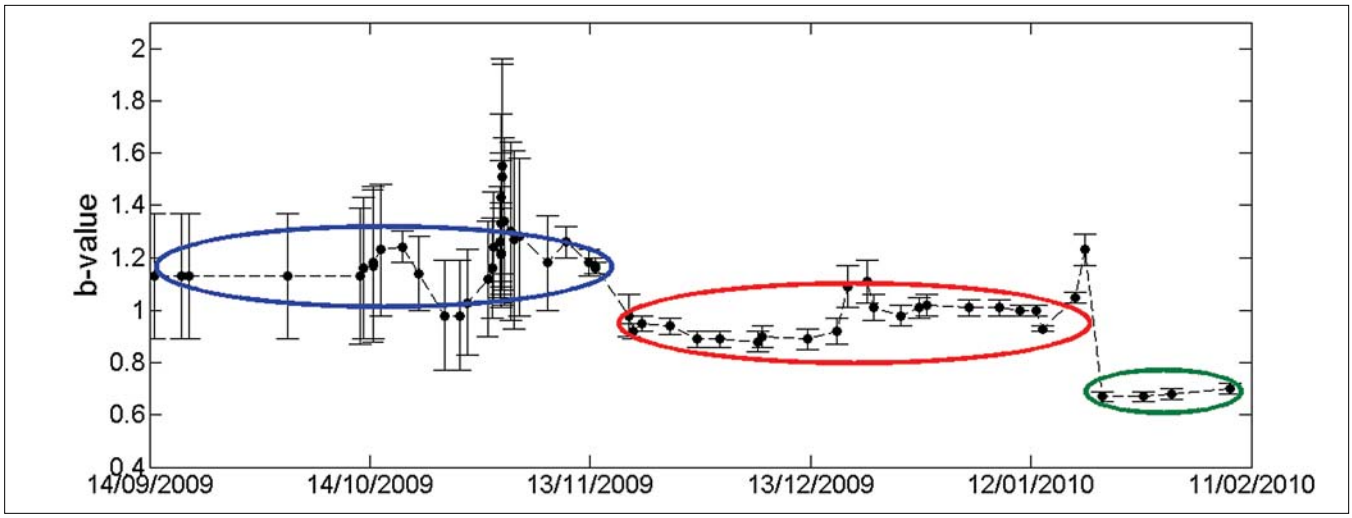

Figure 4. *Temporal evolution of b-values for a heavy-oil data set. Three regimes are visible with initial b-values larger than 1.1 (extensional faulting or opening of fractures) until mid-November 2009, followed by b-values around 1.0, and finally a last stage with values around 0.65 (closing of fractures or compressive faulting), starting at the end of January 2010. The ellipses emphasize the three different stages.*

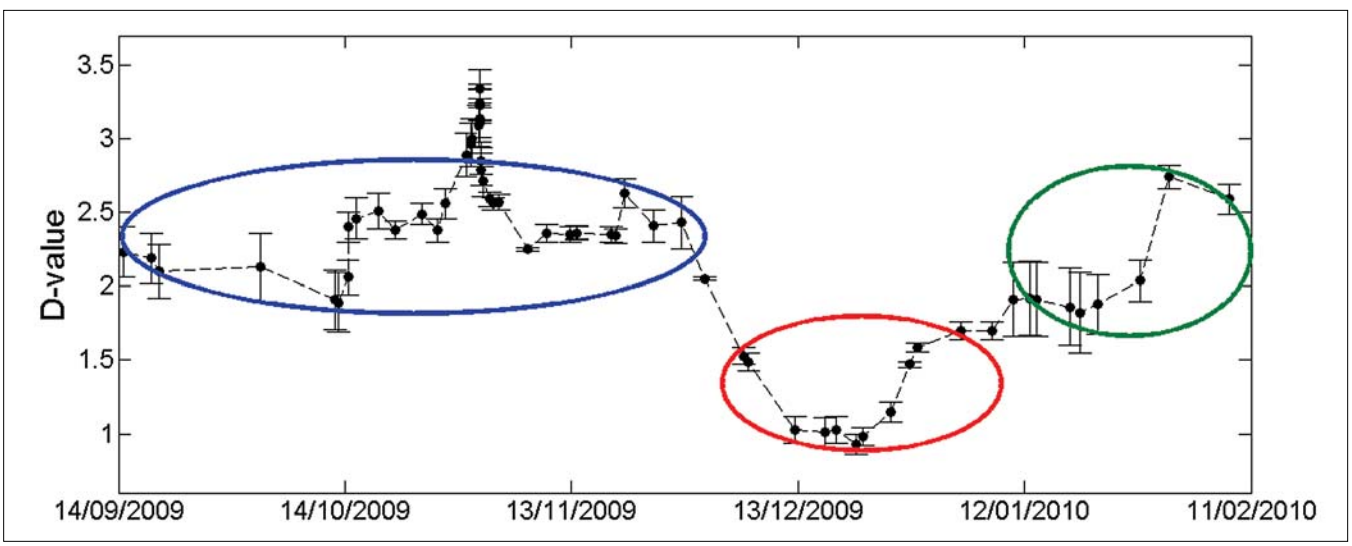

Figure 5. *Temporal evolution of D-values for a heavy-oil data set. No clear correlation exists with the b-values shown in Figure 4, except that the lowest D-values occur in the middle of the second stage, indicating the possible presence of strike-slip faulting. The ellipses emphasize the three different stages.*

ity: experimental and numerical studies and relationship with the b-value: Journal of Geophysical Research B: Solid Earth, **108**, B1, B12044, doi:10.1029/2001JB000680.

Baig, A. and T. Urbancic, 2010, Microseismic moment tensors: a path to understanding frac growth: The Leading Edge, **29**, no. 3, 320–324, doi:10.1190/1.3353729.

Eaton, D. and F. Forouhideh, 2010, Microseismic moment tensors: the good, the bad and the ugly: CSEG Recorder, 44–47.

Fisher, T., S. Hainzl, L. Eisner, S. A. Shapiro, and J. Le Calvez, 2008, Microseismic signatures of hydraulic fracture growth in sediment formations: observations and modeling: Journal of Geophysical Research, **113**, B2, B02307, doi:10.1029/2007JB005070.

Gephart, J. W. and D. W. Forsyth, 1984, An improved method for determining the regional stress tensor using earthquake focal mechanism data: application to the San Fernando earthquake sequence: Journal of Geophysical Research, **89**, no. B11, no. B11, 9305–9320, doi:10.1029/JB089iB11p09305.

Grassberger, P. and I. Procaccia, 1983, Measuring the strangeness of strange attractors: Physica D. Nonlinear Phenomena, **9**, no. 1–2, 189–208, doi:10.1016/0167-2789(83)90298-1.

Gutenberg, B. and C. F. Richter, 1944, Frequency of earthquakes in California: Bulletin of the Seismological Society of America, **34**, no. 4, 185–188.

Helmstetter, A., Y. Y. Kagan, and D. D. Jackson, 2005, Importance of small earthquakes for stress transfers and earthquake triggering: Journal of Geophysical Research, **110**, B5, B05S08, doi:10.1029/2004JB003286.

Henderson, J., I. Main, P. Meredith, and P. Sammonds, 1992, The evolution of seismicity at Parkfield: observation, experiment and a fracture-mechanical interpretation: Journal of Structural Geology, **14**, no. 8-9, 905–913, doi:10.1016/0191-8141(92)90022-O.

Hirata, T., T. Satoh, and K. Ito, 1987, Fractal structure of spatial dis-

tribution of microfracturing in rock: Geophysical Journal of the Royal Astronomical Society, **90**, 369–374.
Huang, J. and D. L. Turcotte, 1988, Fractal distributions of stress and strength and variations of b-value: Earth and Planetary Science Letters, **91**, no. 1-2, 223–230, doi:10.1016/0012-821X(88)90164-1.
Liakopoulou-Morris, F., I. G. Main, B. R. Crawford, and B. G. D. Smart, 1994, Mircoseismic properties of a homogeneous sandstone during fault nucleation and frictional sliding: Geophysical Journal International, **119**, no. 1, 219–230, doi:10.1111/j.1365-246X.1994.tb00923.x.
Lockner, D., 1993, The role of acoustic emission in the study of rock fracture: International Journal of Rock Mechanics and Mining Sciences & Geomechanics Abstracts, **30**, no. 7, 883–899, doi:10.1016/0148-9062(93)90041-B.
McKenzie, D. P., 1969, The relationship between fault plane solutions from earthquakes and the directions of the principal stresses: Bulletin of the Seismological Society of America, **59**, no. 2, 591–601.
Mogi, 1962, Magnitude-frequency relation for elastic shocks accompanying fractures of various materials and some related problems in earthquakes: Bulletin of Earthquake Research Institute Tokyo University, **40**, 831–853.
Rozhko, A. Y., Y. Y. Podladchikov, and F. Renard, 2007, Failure patterns caused by localized rise in pore-fluid overpressure and effective strength of rocks: Geophysical Research Letters, **34**, no. 22, L22304, doi:10.1029/2007GL031696.
Rutledge, J. T., W. S. Phillips, and M. J. Mayerhofer, 2004, Faulting induced by forced fluid injection and fluid flow forced by faulting: An interpretation of hydraulic-fracture microseismicity, Carthage Cotton Valley gas field, Texas: Bulletin of the Seismological Society of America, **94**, no. 5, 1817–1830, doi:10.1785/012003257.
Scholz, C. H., 1968, The frequency-magnitude relation of microfracturing in rock and its relation to earthquakes: Bulletin of the Seismological Society of America, **58**, no. 1, 399–415.
Schorlemmer, D., S. Wiemer, and M. Wyss, 2005, Variations in earthquake-size distribution across different stress regimes: Nature, **437**, no. 7058, 539–542, doi:10.1038/nature04094.
Urbancic, T., C.-I. Trifu, J. M. Long, and R. P. Young, 1992, Spacetime correlations of b values with stress release: Pure and Applied Geophysics, **139**, no. 3-4, 449–462, doi:10.1007/BF00879946.
Urbancic, T., V. Shumila, J. T. Rutledge, and R. J. Zinno, 1999, Determining hydraulic fracture behavior using microseismicity: The 37th U.S. Symposium on Rock Mechanics (USRMS), American Rock Mechanics Association.

Acknowledgments: This work was funded through the Microseismic Industry Consortium. The authors thank all sponsors for their support, and an anonymous company for data licensing and permission to publish.

Corresponding author: grob@ualberta.ca